Available online at www.sciencedirect.com
ScienceDirect
Solid State Communications 146 (2008) 518–521
solid state communications
www.elsevier.com/locate/ssc

Effect of grain boundary on electrical, magnetic and magnetoresistance properties in $La_{2/3}Ca_{1/3}MnO_3/CuMn_2O_4$ composites

Pai Li, Songliu Yuan*, Li Liu, Xueli Wang, Yongqiang Wang, Zhaoming Tian, Jinghua He, Shijun Yuan, Kuili Liu, Shiyan Ying, Chuanhui Wang

Department of Physics, Huazhong University of Science and Technology, Wuhan 430074, People's Republic of China

Received 29 November 2007; received in revised form 25 January 2008; accepted 1 March 2008 by E.V. Sampathkumaran
Available online 8 March 2008

Abstract

Composites of $La_{2/3}Ca_{1/3}MnO_3$ (LCMO)/$CuMn_2O_4$ were synthesized through a sol-gel method. The effect of ferrimagnetic semiconducting $CuMn_2O_4$ on electrical and magnetic properties has been investigated in detail. The structure analysis shows $CuMn_2O_4$ mainly segregates at the grain boundaries of LCMO. With the increasing content of $CuMn_2O_4$, the electrical transport behavior turns from T^2 dependent to T^3 dependent at low temperatures, which suggests electron–phonon and electron–magnon scattering are becoming more important. In addition, the suppression of magnetization and magnetic transition demonstrates the magnetic coupling has a sizeable influence on the composites. A significant enhancement in magnetoresistance (MR) under an applied field 0.3 T is observed over a wide temperature range, which is considered to arise from the enhanced spin-polarized tunneling caused by the addition of $CuMn_2O_4$ at the grain boundaries.

PACS: 71.30.+h; 73.43.Qt; 74.25.Fy; 75.47.Lx

Keywords: A. Composite materials; C. Grain boundary; D. Electrical transport; D. Tunneling

1. Introduction

Recently, extrinsic magnetoresistance (MR) in polycrystalline manganites has attracted considerable attention due to its potential practical application [1–6]. It was found that the extrinsic MR is mainly contributed by the spin-polarized tunneling proposed by Hwang et al. [3], which exhibits a wide temperature range MR under a low field. In order to get better understanding of the underlying physics, a number of studies of polycrystalline manganites with artificial grain boundaries by introducing a second phase have been reported over the past years [3–21], such as $La_{2/3}Ca_{1/3}MnO_3$ (LCMO)/Ag [5], $La_{0.7}Sr_{0.3}MnO_3/Pr_{0.5}Sr_{0.5}MnO_3$ [6], LCMO/$BaTiO_3$ [7], LCMO/CeO_2 [8], LCMO/$NiFe_2O_4$ [9]. The two-phase combination in polycrystalline could be an effective route for achieving better extrinsic MR and suitable for advanced investigation.

In this study, ferrimagnetic semiconducting $CuMn_2O_4$ has been observed as a second phase existing mainly at grain boundaries of LCMO. As $CuMn_2O_4$ is a ferrimagnetic insulator, and its Curie temperature is much lower than that of LCMO, the magnetic coupling should be different in different temperature regions; this would strongly affect magneto-transport behavior and contain abundant physics for advanced investigation. The electrical and magnetic properties of the composites have been investigated in detail, leading to a better understanding of the effect of $CuMn_2O_4$ addition on the broad temperature range MR.

2. Experimental details

Composites of $(1-x)$LCMO/$x$$CuMn_2O_4$ ($x = 0$, 0.04, 0.1, 0.2 and 1) were fabricated through three steps. Firstly, the LCMO and $CuMn_2O_4$ nanopowders were prepared by the sol-gel method [22] taking stoichiometric amounts of La_2O_3, $CaCO_3$, $Mn(CH_3COO)_2{\cdot}4H_2O$ and $Cu(NO_3)_2{\cdot}3H_2O$, each of 99% purity, as starting materials, respectively. The pre-LCMO powders were calcined at 1100 °C for 12 h to form a perovskite phase while the pre-$CuMn_2O_4$ nanopowders were calcined at 350 °C for 3 h to form a spinel phase. Then appropriate molar

* Corresponding author. Tel.: +86 2787556580; fax: +86 2787544525.
E-mail address: yuansl@hust.edu.cn (S. Yuan).

0038-1098/$ - see front matter © 2008 Published by Elsevier Ltd
doi:10.1016/j.ssc.2008.03.006

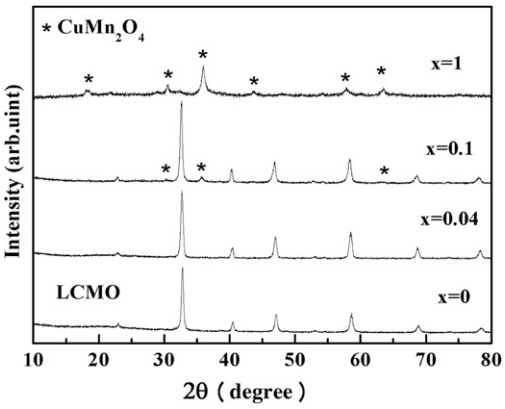

Fig. 1. Room temperature XRD patterns for $(1-x)$LCMO/$x$$CuMn_2O_4$ ($x = 0$, 0.04, 0.1 and 1) system.

amounts of LCMO and $CuMn_2O_4$ nanopowders were mixed properly and a homogeneous powder was formed. Finally, the $(1 - x)$LCMO/$x$$CuMn_2O_4$ powders were pelletized at a pressure of 10 MPa and then sintered at 1000 °C for 2 h. A low sintering temperature for a small duration was chosen to avoid inter-diffusion of LCMO and $CuMn_2O_4$.

The structural characterization of the samples was examined by X-ray diffraction (XRD) at room temperature and the surface morphology was investigated by transmission electronic microscopy (TEM). The electrical transport and magnetoresistance properties were measured with a standard four-probe method in a commercial physical property measurement system.

3. Results and discussion

The room temperature XRD patterns of the composite $(1 - x)$LCMO/$x$$CuMn_2O_4$ ($x = 0$, 0.04, 0.1, 0.2 and 1) are shown in Fig. 1. The patterns show a single orthorhombic perovskite phase for pure LCMO and a spinel phase for $CuMn_2O_4$. For $x = 0.04$, only LCMO patterns are revealed, which could be due to the restriction of the XRD precision. While for $x = 0.01$, both sets of perovskite LCMO and spinel $CuMn_2O_4$ peaks appear in the patterns. It is worth noting that since no other phases were detected in the samples by means of XRD, the interdiffusion between LCMO and $CuMn_2O_4$ could be negligible, therefore it could be expected that $CuMn_2O_4$ mainly segregates at the grain boundaries of the LCMO grains.

Fig. 2 gives the representative TEM photographs for the $x = 0$ and 0.2 composites. From Fig. 2(a), it is revealed that the mean grain size of the LCMO grains is about 400 nm. The large grains in Fig. 2(b) are assigned to the LCMO phases and the small grains are insulating $CuMn_2O_4$, whose average grain size is about 50 nm. Although some small $CuMn_2O_4$ grains are clumped together, the LCMO grains are randomly distributed and well surrounded by small $CuMn_2O_4$ grains. From the structural analysis, we consider that $CuMn_2O_4$ is mainly distributed at grain boundaries of LCMO.

Fig. 3 shows the electrical transport in $(1 - x)$LCMO/x $CuMn_2O_4$ composites. The inset of Fig. 3 shows the $CuMn_2O_4$ concentration dependence of T_{IM} and the peak resistivity.

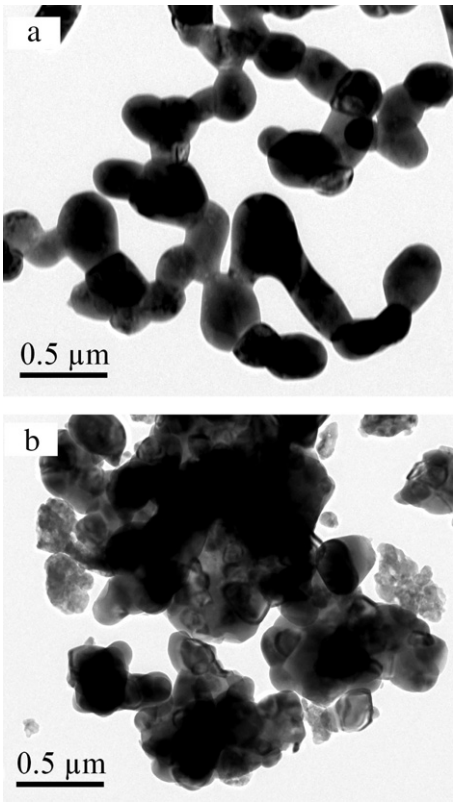

Fig. 2. TEM microphotograph of the $(1 - x)$LCMO/$x$$CuMn_2O_4$ samples with (a) $x = 0$, (b) $x = 0.2$.

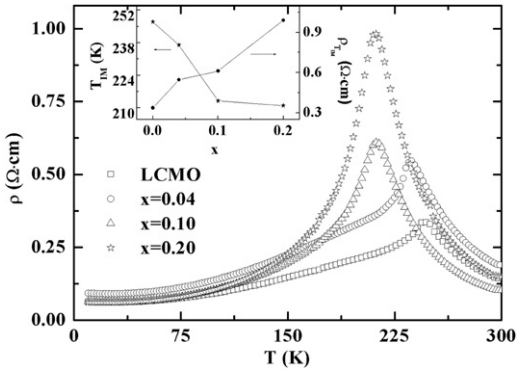

Fig. 3. Temperature dependence of the resistivity for $(1-x)$LCMO/$x$$CuMn_2O_4$ ($x = 0$, 0.04, 0.1 and 0.2). Inset: the peak temperature T_{IM} and peak resistivity ρ_{IM} versus x.

The T_{IM} value decreases from 247 K for pure LCMO to 211 K for the sample with $x = 0.2$. The peak resistivity increases with the increasing content of $CuMn_2O_4$ up to $x = 0.2$. These transport properties are the same with that of the other composites composed of manganite and insulating oxide [23,24].

In order to obtain better understanding of the electrical transport, the mechanism of conduction has been extensively studied. Schiffer et al. [25] had investigated the low temperature resistivity of $La_{0.75}Ca_{0.25}MnO_3$ and found the empirical expression $\rho(T) = \rho_0 + \rho_1 T^{2.5}$ for $T < 0.5T_C$ range. The term ρ_0 is the resistivity derived from domain boundaries and other temperature-independent scattering mechanisms, and the

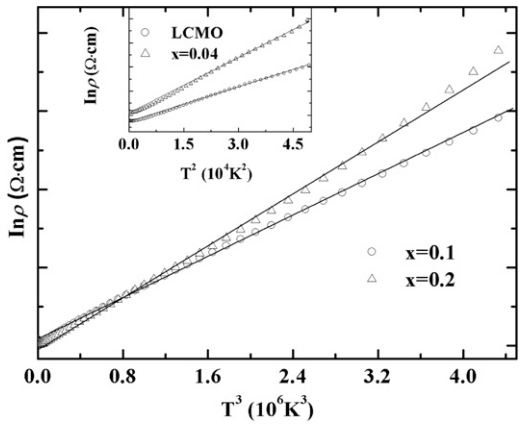

Fig. 4. Relationship between $\ln\rho$ and T^3 for $(1-x)$LCMO/$x$$CuMn_2O_4$ ($x = 0$, 0.04) at zero field. The inset is the relationship between $\ln\rho$ and T^2 for $(1-x)$LCMO/$x$$CuMn_2O_4$ ($x = 0.1$, 0.2). Solid lines indicate the best fits to $\rho_1 T^n$ for ($T < T_{IM}$).

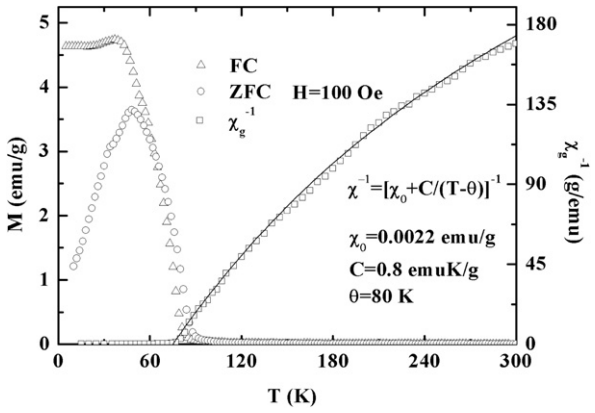

Fig. 5. Temperature dependence of the magnetic suscepbility χ^{-1} and magnetization for ZFC and FC at 0.01 T for $CuMn_2O_4$; Solid line is the best fit for the suscepbility date by $\chi^{-1} = [\chi_0 + C/(T-\theta)]^{-1}$.

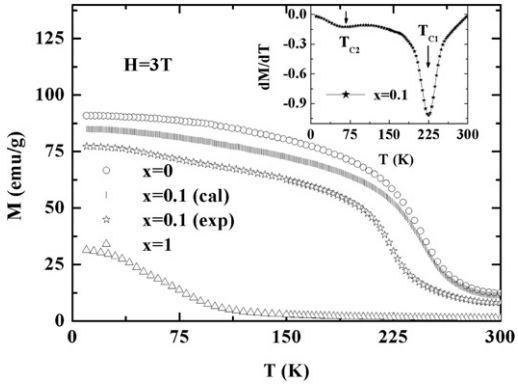

Fig. 6. Magnetization as a function of temperature in an applied field of 5 T for the $(1-x)$LCMO/$x$$CuMn_2O_4$ ($x = 0$, 0.1 and 1) samples. The inset shows Curie temperatures and resistance vs. temperature for $x = 0.1$ sample.

$\rho_1 T^{2.5}$ term is an empirical fit to the data which represents a combination of electron–electron (T^2), electron–phonon (T^5), and electron–magnon scattering ($T^{4.5}$) [26]. We have tried to fit the low temperature resistivity for all the samples by using different exponents for the term $\rho_1 T^n$, but there is no uniform parameter n able to fit all the samples well. The results displays that the term $\rho_1 T^2$ is found to be the best fit for $x = 0$ and 0.04 as seen in the inset of Fig. 4, while the term $\rho_1 T^3$ turns to be the most adequate fit for $x = 0.1$ and 0.2. As a result, it can be inferred that for pure LCMO, electron–electron scattering is the most important factor controlling the low temperature electrical behavior, while for the composites with increasing content of $CuMn_2O_4$, electron–phonon and electron–magnon scattering can not be ignored and seem be of greater importance.

Fig. 5 displays the temperature dependence of the magnetization M for $CuMn_2O_4$ under a low magnetic field 0.01 T. The zero-field-cooling (ZFC) curve shows an obvious peak at $T_F = 48$ K, which is nearly absent under FC (field-cooling) conditions. This result is similar to the previous literature report [27]. The difference between ZFC and FC indicates that some small ferromagnetic ordering is forced on field cooling and it hinges on Cu^{2+}–Mn^{3+} and Cu^{+}–Mn^{4+} interactions, which confirms our sample $CuMn_2O_4$ to be ferrimagnetic. The inverse susceptibility as a function of temperature is shown in Fig. 6 and the susceptibility data can be approximated by $\chi^{-1} = [\chi_0 + C/(T-\theta)]^{-1}$, where χ_0 is a temperature-dependent component of the susceptibility and C is a constant. From the extrapolation of the approximated fitting in Fig. 5, it is clear that the $CuMn_2O_4$ sample shows a PM to ferrimagnetic transition at about 80 K.

In order to get more information about magnetic coupling at the grain boundaries, the magnetic behavior of the samples have been investigated. Fig. 6 presents the temperature dependence of magnetization M for $x = 0$, 0.1 and 1 under an applied field of 3 T. The Curie temperature T_C is defined as the temperature corresponding to the minimum in dM/dT–T curves. The inset shows the derivation of magnetization dM/dT as a function of temperature for $x = 0.1$, as shown in Fig. 6. It obviously presents two different magnetic transitions: T_{C1} derived from the LCMO phase while T_{C2} corresponds to $CuMn_2O_4$, indicating that $CuMn_2O_4$ still retains its individual magnetic phase despite the combination with LCMO. If we assume that there is no spin coupling and interfacial diffusion between neighboring LCMO grains and $CuMn_2O_4$ boundaries, the magnetization M_{LC} for $(1-x)$LCMO/$x$$CuMn_2O_4$ should be as below:

$$M_{LC}(T) = (1-x)\,M_L(T) + x M_C(T) \quad (1)$$

where M_L and M_{C_u} are the magnetization of LCMO and $CuMn_2O_4$, respectively. The predicted $M_{LC}(T)$ is inserted in Fig. 6 for a comparison. The predicted $M_{LC}(T)$–T and measured $M_{LC}(T)$–T curves are similar in shape but differences could not be ignored for the value of magnetization and the magnetic transition temperature. The magnetization value of the measured curve is about 8 emu/g smaller than that of the predicted curve nearly over the whole temperature range. Furthermore, the magnetic transition temperature of the measured curve T_{C1}(225 K) displays an obvious shift to low temperature as compared with the Curie temperature of the predicted curve (250 K). We considered these obvious differences can be attributed to the suppression of the ferromagnetic alignment of Mn ions inside LCMO grains

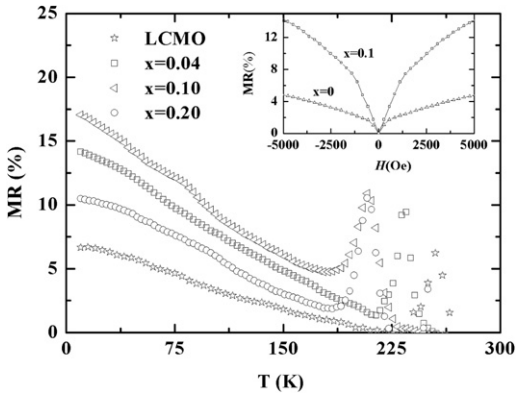

Fig. 7. Temperature dependence of MR for $(1-x)$LCMO/$x$$CuMn_2O_4$ ($x = 0$, 0.04, 0.1, 0.2) at $H = 0.3$ T. Inset: field dependence of MR for $(1-x)$LCMO/$x$$CuMn_2O_4$ ($x = 0$, 0.1) at 90 K.

near the contacting boundaries caused by magnetic disorder attributed to $CuMn_2O_4$.

Fig. 7 presents the temperature-dependent MR curves for the composites of $(1-x)$LCMO/$x$$CuMn_2O_4$ with $x = 0$, 0.04, 0.1, and 0.2 under an applied magnetic field of 0.3 T, respectively. Here MR is calculated by $MR_0(\%) = [\rho(T,0) - \rho(T,H)]/\rho(T,0) \times 100\%$, where $\rho(T,0)$ and $\rho(T,H)$ are resistivity values in zero and applied fields of H. Inset shows field dependence of MR for $(1-x)$LCMO/$x$$CuMn_2O_4$ ($x = 0, 0.1$) at 90 K. All the composites exhibit a MR peak near T_{IM} and this kind of MR is the so-called colossal magnetoresistance (CMR) due to the double exchange mechanism [28]. However, the intrinsic CMR effect in the grains has little influence on MR at low temperatures [3], and what we focus on is the extrinsic MR value for the composites with $CuMn_2O_4$ addition. The results show that extrinsic MR of the composites is much larger than that of pure LCMO. Especially for the $x = 0.1$ sample, the extrinsic MR is nearly two times larger than that of the pure LCMO sample. To the best of our knowledge, the grain boundaries of pure polycrystalline LCMO are mainly due to the imperfect crystallization, which shows an insulating behavior. Consequently, spin-polarized tunneling gives an appropriate explanation for the electrical transport of polycrystalline manganites. We consider there are two aspects strongly affecting the spin-polarized tunneling. One is the thickness of insulator barrier, and the other is the magnetic coupling at the grain boundaries. As a result, the addition of $CuMn_2O_4$ results in increased thickness of the insulating grain boundaries and much stronger magnetic coupling between LCMO and $CuMn_2O_4$ at grain boundaries, which leads to the enhancement of the extrinsic MR.

4. Conclusions

In conclusion, composites of $(1-x)$LCMO/$x$$CuMn_2O_4$ ($x = 0$, 0.04, 0.1, 0.2 and 1) have been fabricated. Microstructural studies show the $CuMn_2O_4$ appears as a separate phase mainly at LCMO grain boundaries for concentrations $x \geq 0.1$. For concentrations $x \leq 0.04$, the X-ray diffraction studies indicate the presence of only the LCMO phase. Our results show that both the electrical transport and magnetic properties are strongly affected by the ferrimagnetic insulating $CuMn_2O_4$ addition. A significant enhancement in extrinsic MR is observed for the composites at a wide temperature range below T_{IM}. Especially for the $x = 0.1$ sample, the extrinsic MR is nearly two times larger than that of the pure LCMO sample. This could be attributed to the enhanced spin-polarized tunneling induced by the modified grain boundaries caused by the $CuMn_2O_4$ addition.

Acknowledgements

This work was supported by National 973 project of China (Grant No. 2006CB921606), by the National Science Foundation of China (Grant No. 10574049), and by the Foundation from the ministry of the National Education (Grant No. 20060487011).

References

[1] L.E. Hueso, J. Rivas, F. Rivadula, M.A. Lopez-Quintela, J. Appl. Phys. 86 (2000) 3881.
[2] X.L. Wang, S.X. Dou, H.K. Liu, M. Ionescu, B. Zeimetz, Appl. Phys. Lett. 73 (1998) 396.
[3] H.Y. Hwang, S.W. Cheong, N.P. Ong, B. Batiogg, Phys. Rev. Lett. 77 (1996) 2041.
[4] Y.H. Huang, C.H. Yan, F. Luo, W. Song, Z.M. Wang, C.S. Liao, Appl. Phys. Lett. 81 (2002) 1.
[5] J.M. Liu, G.L. Yuan, H. Sang, Z.C. Wu, X.Y. Chen, Z.G. Liu, Y.W. Du, Q. Huang, C.K. Ong, Appl. Phys. Lett. 78 (2001) 1110.
[6] G.M. Ren, S.L. Yuan, G.Q. Yu, J.H. Miao, X. Xiao, H.G. Guan, Y.Q. Wang, S.Y. Yin, J. Phys. D: Appl. Phys. 39 (2006) 4867.
[7] L.D. Yao, W. Zhang, J.S. Zhang, H. Yang, F.Y. Li, Z.X. Liu, C.Q. Jin, R.C. Yu, J. Appl. Phys. 101 (2007) 063905.
[8] B.B. Nayak, S. Vitta, D. Bahadur, Mater. Sci. Eng. B 139 (2007) 171.
[9] A. Gupta, J.Z. Sun, J. Magn. Magn. Mater. 200 (1999) 24.
[10] J.M. Liu, G.L. Yuna, X.Y. Chen, Z.G. Liu, Y.W. Du, Q. Hwang, J. Li, X.Y. Xu, C.K. Ong, Appl. Phys. A 73 (2001) 625.
[11] D.K. Petrov, L. Krusin-Elbaum, J.Z. Sun, C. Field, P.R. Duncombe, Appl. Phys. Lett. 75 (1999) 995.
[12] D. Das, P. Chowdhury, R.N. Das, C.M. Srivastava, A.K. Nigam, D. Bahadur, J. Magn. Magn. Mater. 238 (2002) 178.
[13] B.S. Kang, H. Wang, J.L. MacManus-Driscoll, Q.X. Jia, I. Mihut, J.B. Betts, Appl. Phys. Lett. 88 (2006) 192514.
[14] Y.H. Huang, X. Chen, Z.M. Wang, C.-S. Liao, C.H. Yan, H.W. Zhao, B.G. Shen, J. Appl. Phys. 91 (2002) 7733.
[15] C.H. Yan, Y.H. Huang, X. Chen, C.S. Liao, Z.M. Wang, J. Phys.: Condens. Matter 14 (2002) 9607.
[16] G. Dezanneau, A. Sin, H. Roussel, H. Vincent, M. Audier, Solid State Commun. 121 (2002) 133.
[17] F. Luo, S. Wei, Z.M. Wang, C.H. Yan, Appl. Phys. Lett. 84 (2004) 1719.
[18] J. Kumar, P.K. Siwach, R.K. Singh, H.K. Singh, R. Singh, O.N. Srivastava, J. Magn. Magn. Mater. 299 (2006) 155.
[19] M. Eshraghi, H. Salamati, P. Kameli, J. Alloys Compd. 437 (2007) 22.
[20] S. Karmakar, S. Taran1, B.K. Chaudhuri, H. Sakata, C.P. Sun, C.L. Huang, H.D. Yang, J. Phys. D: Appl. Phys. 38 (2005) 3757.
[21] Z.G. Sheng, Y.P. Sun, X.B. Zhu, W.H. Song, P. Yan, J. Phys. D: Appl. Phys. 40 (2007) 3300.
[22] R.D. Sanchez, J. Rivas, C. Vazquez, M.A. Lopez-Quintela, M.T. Causa, M. Tovar, S. Oseroff, Appl. Phys. Lett. 68 (1996) 134.
[23] L.I. Balcells, A.E. Carrillo, B. Martinez, J. Fontcuberta, Appl. Phys. Lett. 74 (1999) 4014.
[24] D. Das, C.M. Srivastava, D. Bahadur, A.K. Nigam, S.K. Malik, J. Phys. Condens. Matter 16 (2004) 4089.
[25] P. Schiffer, A.P. Ramirez, W. Bao, S.W. Cheong, Phys. Rev. Lett. 75 (1995) 3336.
[26] K. Kubo, N. Ohata, J. Phys. Soc. Jpn. 33 (1972) 21.7.
[27] A. Waskowska, L. Gerward, J. Staun Olsen, S. Steenstrup, E. Talik, J. Phys.: Condens. Matter 13 (2001) 2549.
[28] C. Zener, Phys. Rev. B 82 (1951) 403.